Assessment of the Far-Field Exergy Balance Method for Industrial Aerodynamic and Aerothermal Applications

Myles Morelli, Simon Trapier, Luis Lopez de Vega, William Thollet, Ilias Petropoulos, Ilyès Berhouni

Association Aéronautique et Astronautique de France

58th 3AF International Conference on Applied Aerodynamics
27 — 29 March 2024, Orléans – France

AERO2024-37

Assessment of the Far-Field Exergy Balance Method for Industrial Aerodynamic and Aerothermal Applications

Myles Morelli[(1)], Simon Trapier[(1)], Luis Lopez de Vega[(1)], William Thollet[(1)], Ilias Petropoulos[(2)] and Ilyès Berhouni [(2)]
[(1)]*Airbus Operations S.A.S., 316 route de Bayonne, 31060 Toulouse, France,*
Email: name.surname@airbus.com
[(2)]*ONERA, 8 rue des Vertugadins, 92190 Meudon, France,*
Email: name.surname@onera.fr

ABSTRACT

This work evaluates the far-field exergy balance method in the context of industrial aerodynamic and aerothermal applications pertinent to prospective aircraft architectures and technologies. The utilization of the exergy balance method facilitates the breakdown of aircraft performance into distinct physical features and properties inherent in the aerodynamic flow. The investigation focuses on open fan and heat exchanger configurations, representative of components integral to potential future propulsive systems. The findings contribute to a deeper understanding of the intricacies associated with the interaction between aerodynamic components and thermal processes, thereby informing the design and optimization of future aircraft propulsion systems.

1. INTRODUCTION

The need for improving numerical modelling techniques has arisen with the goal towards finding impactful solutions that can help deliver sustainable aircraft and, ultimately, climate-neutral aviation. While novel future aircraft architectures and technologies are promising, they require investment in the development of new tools to accurately model the highly challenging and complex aerodynamic and aerothermal physics associated with them. A notable example is the prediction of aircraft drag, where the limitations of current methodologies are underscored by the work of Drela [1]. This research highlights the existing constraints in predicting the drag associated with potential future aircraft architectures and technologies through the application of traditional far-field drag breakdown methods.

The exergy balance method, originally proposed for the analysis of aerodynamic flows by Arntz et al. [2, 3], constitutes a new approach to assess the aeropropulsive and aerothermal performance of aircraft or aircraft components, and connect this performance to physical features and properties of the aerodynamic flow. The FFX (Far-Field Exergy) software, developed at ONERA, implements this approach for analyzing results of CFD simulations through integrals in the flowfield volume [4]. This method provides a novel approach to the assessment of aircraft performance, alternative to the classical concepts of drag and thrust. It is of particular interest when drag and thrust cannot be easily separated, for instance when the propulsion system and the airframe are in close interaction, or when aerothermal effects play a significant role.

The research project IDEFFIX, conducted from 2020 to 2023 and supported by the French Directorate General for Civil Aviation (DGAC), was aimed at developing this tool in order to provide new capabilities for designing future aircraft architectures and engines technologies [5]. As a contribution to this project, Airbus has applied FFX to several industrially-relevant aerodynamic and aerothermal cases. The present paper summarizes the results of a part of these applications and their main conclusions, focusing on two types of configurations: (1) open fan engines and (2) heat exchangers.

The remainder of the paper is structured as follows: Sec. 2 introduces the far-field exergy method, Sec. 3 & 4 respectively discuss the aerodynamic and aerothermal applications studied, and Sec. 5 summarizes the key conclusions from this work.

2. EXERGY ANALYSIS

2.1 Exergy Definition

Exergy is defined as the maximum amount of work that can be extracted from a system as it is brought into equilibrium with a reservoir (in this case corresponding to its thermodynamic dead state) through reversible processes. It can be thought of as a measure of the usefulness or quality of energy. While assuming a perfect gas and neglecting gravitational potential energy, exergy χ can be expressed as:

$$\chi \triangleq \delta e + p_\infty \delta\left(\frac{1}{\rho}\right) - T_\infty \delta s + \frac{1}{2}\left(\mathbf{V}-\mathbf{V}_\infty\right)^2 \qquad (1)$$

where ρ is static density, e is specific internal energy, T is static temperature, p is static pressure and s is specific entropy. In addition, $\delta(\bullet) = (\bullet) - (\bullet)_\infty$ is the perturbation of a quantity with respect to the reference state (denoted by the subscript $_\infty$). Eq. (1) corresponds to a recently-proposed corrected adaptation of the exergy definition for aerodynamic flows [6], in particular considering a dead state that is in motion at a velocity $\mathbf{V}_\infty \neq \mathbf{0}$.

2.2 Exergy Balance Formulation

This work evaluates the aerodynamic performance of aircraft using flow solutions obtained computationally using the Reynolds-averaged Navier-Stokes (RANS) equations. Over the last decades, ONERA has been working on the development of specialized methods for the accurate performance evaluation of aircraft configurations based on far-field drag analysis [7, 8, 9]. In this context, although originally oriented towards very innovative configurations, a balance of exergy for the analysis of aerodynamic flows was more recently introduced by Artnz et al. [2, 3]. This work has since been investigated on different aspects, for example concerning the analysis of experimental data [10]. More recently, the exergy balance formulation has been extended to the analysis of rotating flows [4] and turbomachinery applications in particular [11, 12].

In the present work, the far-field exergy balance method introduced by Berhouni et al. [11, 6] has been utilized for evaluating flow solutions. This specific exergy balance formulation is suitable for a wide spectrum of aerodynamics or aerothermal applications, and especially for the evaluation of rotating bodies such as propellers. An illustration of the exergy balance for a generic open fan configuration is displayed in Fig. 1.

The formulation is obtained by expressing a balance of exergy in a control volume of fluid surrounding an aircraft in motion. The upstream and lateral boundaries of this volume may extend far from the aircraft, whereas its downstream limit is a transverse plane, the x-coordinate of which is noted x_{tp}. This system is thermodynamically open, as it exchanges mass, work and heat with its surroundings, across its boundaries. For the sake of brevity, the following presentation of the formulation will be limited to its compact form. The complete expressions of the different terms of the formulations can be found in [11]. As such, the compact form of the exergy balance can be written as:

$$\dot{\mathrm{X}}_r + \dot{\mathrm{X}}_{tf} = \dot{\mathrm{X}}_{tr} + \dot{\mathrm{X}}_m + \dot{\mathrm{X}}_{th} + \dot{\mathrm{A}}_\phi + \dot{\mathrm{A}}_{\nabla T} + \dot{\mathrm{A}}_w \qquad (2)$$

With respect to [11], unsteady terms in the above equation have been omitted because this paper is focused on the analysis of steady flow solutions. Wall boundaries are considered adiabatic, whereas the heat flux and the rate of work of viscous forces on the volumes have been found to have a negligible contribution to the overall balance in practice.

The left hand side of the exergy balance described in Eq. (2) represents the inflow of exergy into the system. The term $\dot{\mathrm{X}}_r$ is the flux of mechanical exergy that is transferred to the fluid through rotating wall boundaries and is equal to the rotor shaft power. Then, $\dot{\mathrm{X}}_{tf}$ is the inflow of exergy introduced by the throughflow boundaries on the aircraft. These are commonly source terms or permeable boundary conditions modeling the propulsion system interfaces.

The right hand side of the exergy balance described in Eq. (2) generally represents the use, outflow, or irreversible loss of exergy from the control volume. First of all, the term $\dot{\mathrm{X}}_{tr}$ is the part of the provided exergy flux that is converted to effective thrust (overall axial streamwise force) for a configuration translating at a velocity $\mathbf{V}_\infty$.

The term $\dot{\mathrm{X}}_m$ denotes the overall mechanical exergy outflow from the control volume and can be further decomposed into three separate useful terms:

$$\dot{\mathrm{X}}_m = \dot{E}_u + \dot{E}_{vw} + \dot{E}_p \qquad (3)$$

where, $\dot{E}_u$ is the axial kinetic perturbation energy outflow in the streamwise direction and may be associated with the wake or the jet of the propulsion system. $\dot{E}_{vw}$ is then the corresponding transverse kinetic perturbation energy outflow and is commonly associated with vortical flow structures, whereas $\dot{E}_p$ is finally the contribution of the rate of work of surface forces related to the aforementioned kinetic energy perturbations.

The term $\dot{\mathrm{X}}_{th}$ describes the thermocompressible exergy outflow. It can also be referred to as the static exergy outflow, as it corresponds to the static part of the exergy definition of Eq. (1). The decomposition of this term using the exergy definition itself, although straightforward, is often impractical. This is due to the fact that significant reversible exchanges may occur between the compressible contributions to this term and $\dot{\mathrm{X}}_m$. In order to resolve this shortcoming, this term is decomposed using a particular approach described in [13, 11]. This is based on fix-

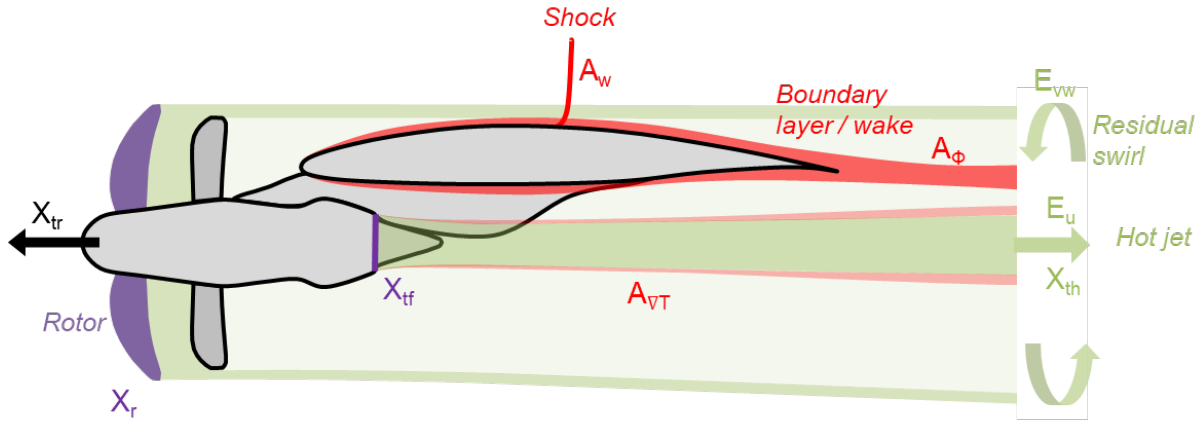

Figure 1: Schematic illustration of the exergy balance for a generic open fan configuration.

ing a specific ideal path for the recovery of exergy, based on an isentropic expansion and a reversible isobaric heat exchange. As such, $\dot{X}_{th}$ is decomposed as:

$$\dot{X}_{th} = \dot{X}_{thse} + \dot{X}_{th\delta s} \tag{4}$$

with $\dot{X}_{thse}$ corresponding to the compressible contribution to $\dot{X}_{th}$ and $\dot{X}_{th\delta s}$ corresponding to the purely thermal one. Using Eqs. (3)-(4), we can express an overall mechanically-recoverable exergy flux (e.g. by a turbine) as $\dot{X}_{mr} = \dot{X}_m + \dot{X}_{thse}$. On the other hand, $\dot{X}_{th\delta s}$ represents the remainder of the overall exergy flux which is only thermally-recoverable by a heat engine (a Carnot machine in the ideal case).

The last three terms in Eq. (2) represent the total rate of exergy dissipation, or equivalently anergy generation, by irreversible processes. Its three components $\dot{A}_\phi$, $\dot{A}_{\nabla T}$ and $\dot{A}_w$ are respectively the anergy generation due to viscous effects, due to thermal mixing and due to the presence of shockwaves.

Overall, the balance of Eq. (2) expresses that not all of the exergy provided to the flow by the rotor ($\dot{X}_r$) or the propulsion system interfaces ($\dot{X}_{tf}$) is converted into effective thrust ($\dot{X}_{tr}$). This is because one portion of it is irreversibly dissipated ($\dot{A}_\phi + \dot{A}_{\nabla T} + \dot{A}_w$), whereas another exits the control volume in the form of mechanical or thermocompressible exergy outflow ($\dot{X}_m + \dot{X}_{th}$). The latter portion is recoverable and can thus theoretically be converted to useful work by a turbine, stator or a wake-recovery device. In the absence of such a device however, this portion will be dissipated by irreversible effects downstream (i.e. a reduction of $\dot{X}_m, \dot{X}_{th}$ and an increase of $\dot{A}_\phi, \dot{A}_{\nabla T}, \dot{A}_w$). In other words, this balance formulation provides a decomposition of the provided exergy which is not converted into effective thrust. Through this decomposition, it provides a quantification of the impact of the aforementioned individual physical phenomena on the overall aircraft performance.

In practice, steady flow solutions involving rotating components such as propellers are often computed in a rotating frame of reference (e.g. attached to the blades). In these cases, the control volume follows the rotation of the fluid volume and thus appears fixed in this frame of reference. All terms in the balance equations are projected in the rotating reference frame, but it should be noted that for a zero entrainment velocity the above balance is simplified to its inertial-frame counterpart. This is an important attribute which allows the uniform treatment of rotating and fixed components. Last, single-blade channel computations may correspond to sectors of a different azimuthal size across mixing plane boundary conditions. For such cases, the exergy balance corresponds to the complete 360° configuration in order to ensure that it is consistent across the mixing plane interface.

In the following results, terms of the exergy balance will be expressed in non-dimensional coefficients $C(\bullet) = (\bullet)/(0.5\rho_\infty V_\infty^3 S_{ref})$, with their values given in power counts (10^{-4}).

The exergy-balance-based analyses of the present paper have been carried out using the *FFX* far-field exergy analysis software developed at ONERA. This software is closely coupled with the ONERA Cassiopée pre-/post-processing library [14] and has been applied to a variety of academic and complex cases over the recent years (Ref. [11] and references therein). *FFX* can accurately analyse finite-volume CFD solutions on structured, unstructured or overset (Chimera) grids, with the solution computed at cell centers or at vertices. In the present work, it has been used for the analysis of solutions computed by two different CFD solvers used at Airbus (elsA [15] and CODA [16]).

3. AERODYNAMIC APPLICATION

The Open Fan concept is a single-stage, unducted engine architecture, enabling much larger fan diameters and bypass ratios than classical turbofans. The associated

gains in propulsive efficiency make this type of engine a promising candidate for powering a next generation of passenger aircraft.

The distinctive characteristics of the Open Fan architecture involve a rotating array of blades, referred to as the *"rotor"*, responsible for a substantial portion of the thrust generation. Additionally, a stationary array of blades, denoted as the *"stator"*, is incorporated to recover the swirl induced by the rotor, thereby contributing to the generation of supplementary thrust.

3.1 Configuration

In the frame of the INPRO research project, Safran has designed aerodynamic shapes for a model Open Fan, which were shared with ONERA and Airbus as a basis for common research activities. CFD computations have been conducted on these shapes and post-processed using FFX. The specific configuration under investigation involved an isolated engine devoid of any pylon or aircraft. An Open Fan configuration representative of the one studied in this work is shown in Fig. 2. The objectives were twofold: (1) leverage the exergy analysis provided by FFX to gain a more profound understanding of the characteristics of the aerodynamic flow around an open fan configuration and quantify their influence on the overall performance, as well as (2) evaluate the capability of various rotor and stator blade modelling approaches to predict the overall propulsive performance of the engine.

Figure 2: Image of the RISE open fan configuration similar to the geometry assessed in this work. Image courtesy of CFM International.

3.2 Modelling

The isolated engine was simulated using three different CFD approaches. All three methodologies employed steady RANS computations; however, varying degrees of modeling fidelity were employed to characterize the rotor and stator blades.

- **Mixing plane:** In this method, the three-dimensional geometry of the rotor and stator blades is physically represented in the simulation. However, only one blade from each row is represented, utilizing periodic boundary conditions to relax the computational mesh. This method is considered as the *"single-passage"* approach. The rotor is computed within a rotating frame of reference, the stator in a fixed frame, and a *"mixing-plane"* boundary is employed to azimuthally average flow variables, facilitating information exchange between the two and allowing to perform steady-state CFD simulations in both domains. The structured-grid solver of the elsA CFD code [15], was used for mixing plane computations.

- **Body Force Modelling (BFM):** In this approach, the three-dimensional geometry of the blades is not represented. Instead, the impact of the open fan propulsion on the flow is modeled through source terms derived from the blade geometry, which are then applied to the flow equations in the area swept by blades [17]. BFM computations were conducted using the new-generation CFD solver CODA [16].

- **Virtual Blade Modelling (VBM):** In this approach, the influence of the blades is also represented through source terms, computed from lift and drag polars of the blade section airfoils, and applied in one single layer of cells in the mesh [18]. VBM computations were performed using the new-generation CFD solver CODA [16].

The mixing plane fully resolves the three-dimensional blade geometry and is considered as the highest-fidelity modelling approach among the ones mentioned above. As a result, it is used as a reference to validate the two alternative reduced-order model approaches based on source terms.

3.3 Results

The evolution, along the flow direction axis, of the main terms of the FFX exergy balance are displayed in Fig. 3. This evolution highlights the main characteristics of the flow around the open fan. The propulsive energy, $C\dot{X}_r$, is delivered to the flow by the rotor blades. However, not all of this energy is converted to useful thrust shown as $C\dot{X}_{tr}$.

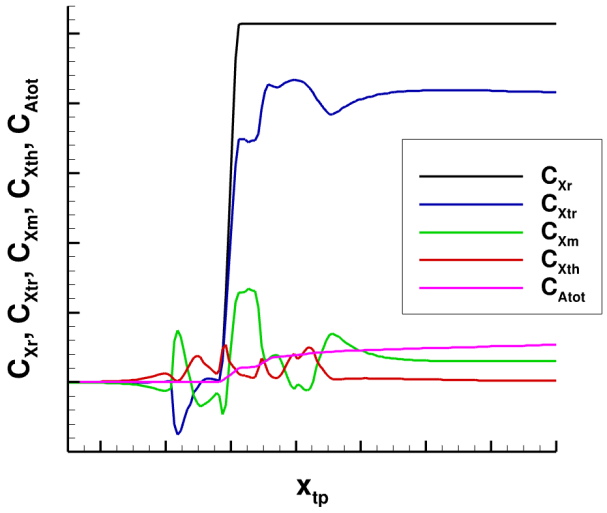

Figure 3: Streamwise evolution of the main terms of the exergy balance for the open fan configuration using the single-passage mixing plane modelling approach.

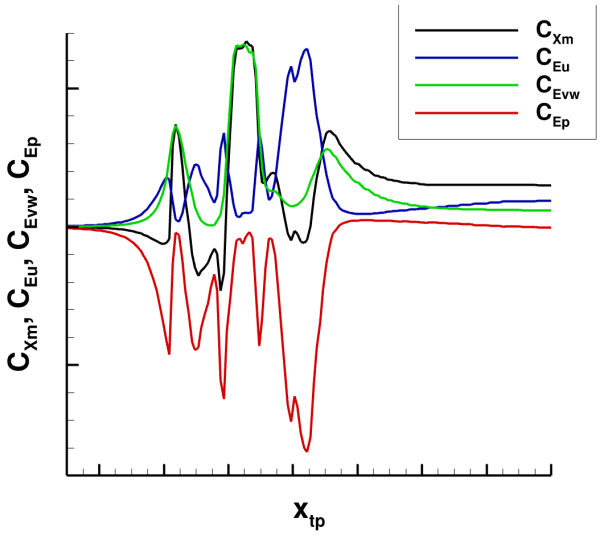

Figure 4: Decomposition of the mechanical exergy outflow term, $C\dot{\mathrm{X}}_m$, into the three energy outflow components $C\dot{E}_u$, $C\dot{E}_{vw}$ and $C\dot{E}_p$ for the open fan configuration using the single passage mixing plane modelling approach.

Part of $C\dot{\mathrm{X}}_r$ is converted to anergy due to dissipative phenomena near the blade walls, their wakes or within shockwaves, $C\dot{\mathrm{A}}_{tot} = C\dot{\mathrm{A}}_{\phi} + C\dot{\mathrm{A}}_{\nabla T} + C\dot{\mathrm{A}}_{w}$ whereas a significant part of it is communicated to the flow as mechanical or thermocompressible exergy $C\dot{\mathrm{X}}_m$ and $C\dot{\mathrm{X}}_{th}$. The latter is of a lower magnitude downstream of the body, as compressible effects associated to the body are of second order of magnitude with respect to the other terms.

While crossing the stator, some additional anergy is produced that further increases $C\dot{\mathrm{A}}_{tot}$. On the other hand, the mechanical exergy of the flow, $C\dot{\mathrm{X}}_m$, decreases, and is converted to used exergy, $C\dot{\mathrm{X}}_{tr}$. This reflects the fact that the stator has recovered a significant portion of the swirl generated by the rotor and converted it to thrust, thus increasing the overall propulsive efficiency of the open fan engine. Part of the variations of thermocompressible exergy outflow $C\dot{\mathrm{X}}_{th}$ appear to be opposite to those of $C\dot{\mathrm{X}}_m$, which suggests that these variations may be related to compressible effects.

Fig. 4 further details the analysis by splitting the mechanical exergy, $C\dot{\mathrm{X}}_m$, into its three components $C\dot{E}_u$, $C\dot{E}_{vw}$ and $C\dot{E}_p$. It shows that the decrease of $C\dot{\mathrm{X}}_m$ through the stator is correlated to the decrease of $C\dot{E}_{vw}$, the transverse kinetic energy outflow. This confirms that the main action of the stator is to recover the swirl of the flow. Also, significant variations of $C\dot{E}_p$ are observed close to the engine skin, with an overall opposite behaviour with respect to $C\dot{E}_u$, but they diminish further downstream as pressure and velocity fluctuations diminish as well. These variations are partially related to compressible reversible exchanges between mechanical and internal energy.

Fig. 5 shows the streamwise evolution of the main exergy balance terms in the BFM and VBM results, which can be compared to the mixing plane results from Fig. 3. It can be observed that the qualitative evolution of all terms is similar to the one from Fig. 3, meaning that all main physical phenomena in the flow have been represented by both models. The main noticeable difference is that the increase of overall anergy ($C\dot{\mathrm{A}}_{tot}$) through the rotor and stator blades is overestimated in the VBM results compared to the BFM and the mixing plane results, suggesting that the loss model in the VBM could be improved. The one in the BFM on the other hand provides a better agreement with the reference single-passage approach.

Focusing again on the components of mechanical exergy, $C\dot{\mathrm{X}}_m$, Fig. 6 shows another discrepancy between the computational approaches. The transverse kinetic exergy, $C\dot{E}_{vw}$, reduces to nearly zero downstream of the stator for the VBM and BFM results. This indicates that the stator effectively reduces the residual swirl $C\dot{E}_{vw}$ introduced by the rotor, a reduction which is less significant for the case of the mixing plane reference computation, as shown in Fig. 4. The largest portion of this swirl reduction is converted to effective thrust, depicted as an increase of $C\dot{\mathrm{X}}_{tr}$, whereas the rest of the exergy flux is irreversibly dissipated due to the stator blades (boundary layers, wakes and eventually shockwaves). Efficient stator designs are expected to maximize the conversion of the residual swirl into thrust while at the same time minimizing these irreversible losses.

To gain a deeper understanding of these distinctions, we can refer to Fig. 7, which presents the local fluxes

of $C\dot{X}_m$, $C\dot{E}_u$, $C\dot{E}_{vw}$, and $C\dot{E}_p$ on a x_{tp} plane situated downstream of the stator. The results obtained from the mixing plane computation have been azimuthally averaged to facilitate direct comparability with the BFM and VBM models. The contour reveals that the predictions of mechanical exergy, $C\dot{X}_m$, displayed in Figs. 7a, 7b, 7c are in relatively good agreement across all modeling approaches. However, a closer examination of the different energy terms indicates that the BFM aligns more closely with the single-passage computations than the VBM. Specifically, the VBM tends to overestimate both $C\dot{E}_u$ and $C\dot{E}_p$ as shown in Figs. 7d & 7j. The observed concordance in $C\dot{X}_m$ among the various modeling approaches seems to arise from a compensation effect, wherein the two overestimations of $C\dot{E}_u$ and $C\dot{E}_p$ from the VBM counterbalance each other owing to their opposite signs. Furthermore, these visualizations (and those of the term $C\dot{E}_{vw}$ in particular) illustrate that the single-passage mixing plane results displayed in Fig. 7i accurately consider blade tip effects, including the generation of blade tip vortices. In contrast, as shown in Figs. 7g & 7h this effect is not captured by either the BFM or VBM approach, as it is not accounted for in their respective modeling. This effect is related to the previously-discussed underestimation of the residual $C\dot{E}_{vw}$ for the VBM and BFM cases.

3.4 Conclusion

The results of the FFX analysis enabled the validation of the ability of BFM and VBM to represent the flow around an open fan. Additionally, the analysis offered insights into the limitations of these models, highlighting specific aspects of the flow physics that require better representation to enhance their capability for accurately predicting propulsive performance.

4. AEROTHERMAL APPLICATION

One of the challenges associated with electric propulsion systems for aircraft is the requirement for effective heat exchangers. Efficient thermal management is crucial in electric propulsion to dissipate heat generated during high-power operations, such as takeoff and climb. Developing advanced heat exchanger technologies becomes imperative to address this challenge and enhance the overall efficiency and reliability of electric propulsion systems in aviation. Moreover, there may be strong interaction effects between heat exchangers and propeller propulsion systems that will impact propeller design and integration. The exergy balance method used in the present work includes the analysis of mechanical, thermal and compressible effects in a single formulation and therefore is particularly interesting for the study of such aspects.

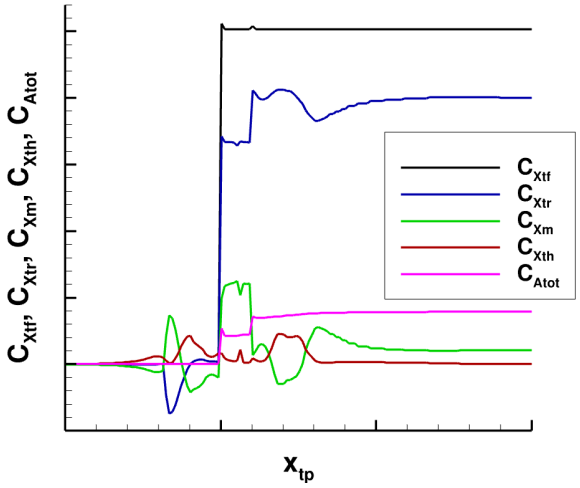

(a) VBM.

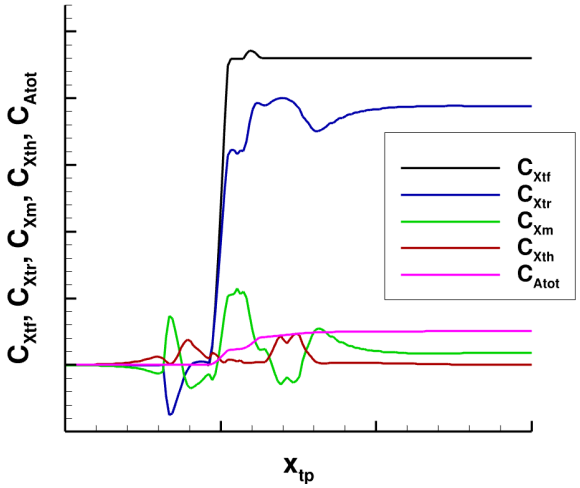

(b) BFM.

Figure 5: Streamwise evolution of the main terms from the exergy balance for the open fan configuration using the VBM and BFM modelling approaches.

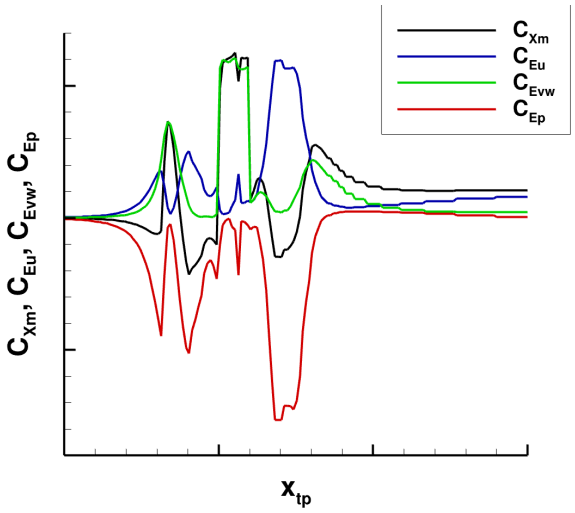

(a) VBM.

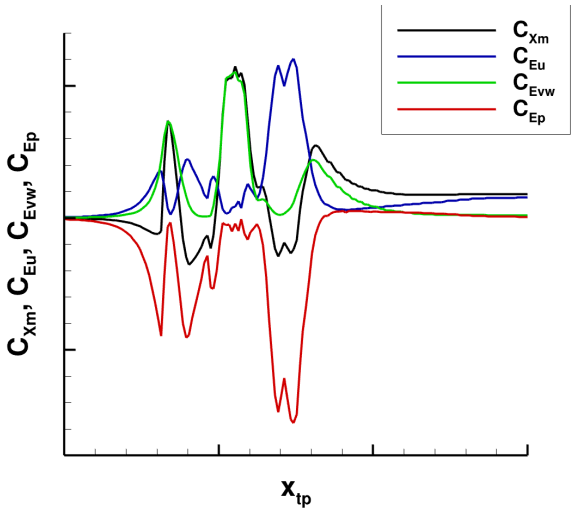

(b) BFM.

Figure 6: Decomposition of the mechanical exergy outflow terms into the three components $C\dot{E}_u$, $C\dot{E}_{vw}$ and $C\dot{E}_p$ for the open fan configuration using the VBM and BFM.

4.1 Configuration

This work simulates a channel flow with a squared section and a heat exchanger. This study focuses on the most basic configuration to gain a preliminary understanding of the fundamental impacts of heat exchangers on the thermal terms in the exergy balance. The basic heat exchanger configuration described is shown in Fig. 8. It displays that the heat exchanger warms the flow uniformly in the z-direction, however, there is a non-uniform heating applied in the y-direction.

4.2 Modelling

The aerodynamics and aerothermal coupling of the heat exchanger was simulated using the next generation CFD solver CODA [16]. The Body Force Modelling (BFM) approach was used to introduce temperature variation in the flow solution through the use of momentum and energy source terms.

4.3 Results

The evolution of the exergy outflow due to the heat exchanger is shown in Fig. 9. The results clearly depict the x_{tp} location where the heat exchanger injects thermal energy into the flow. This is represented by the step increase in the term $C\dot{X}_{tf}$ and is introduced by source terms from the BFM. As one would expect, the contribution from the terms $C\dot{X}_{tr}$ and $C\dot{X}_m$ is of a lower magnitude since the static heat exchanger is not designed to provide propulsive force by accelerating the flow. Furthermore, the exergy balance identifies that the dominant contribution is in terms of $C\dot{X}_{th}$, which highlights that most of the exergy outflow is of a thermocompressible nature.

In internal flows it is often more meaningful to investigate the sum $C\dot{X}_{tr} + C\dot{X}_m$ rather than the two terms independently (equivalent to the $C\dot{X}_m$ value for $\mathbf{V}_\infty = \mathbf{0}$), as the sum corresponds to the perceived flux for a dead state that is not in motion [6, 11]. In the present case, the reduction of this sum across the source terms indicates that the effect of this heat exchanger model is an introduction of a thermocompressible exergy flux and a reduction of the overall mechanical one (i.e. related to drag generation). This explains why the overall exergy inflow by the source term $C\dot{X}_{tf}$ is lower than the thermocompressible exergy flux $C\dot{X}_{th}$ itself. Such an interpretation could be more straightforward on realistic cases by decomposing the $C\dot{X}_{tf}$ term (cf. discussion in [11]).

To further understand the thermocompressible term, $C\dot{X}_{th}$, it can be decomposed into $C\dot{X}_{thse}$ and $C\dot{X}_{th\delta s}$ (cf. Eq. (4)) which respectively represent the compressible and purely thermal contributions [13]. The contribution from these components is shown in Fig. 10 where the y-axis is shown in logarithmic scale to display difference in order of magnitude between the terms. The results

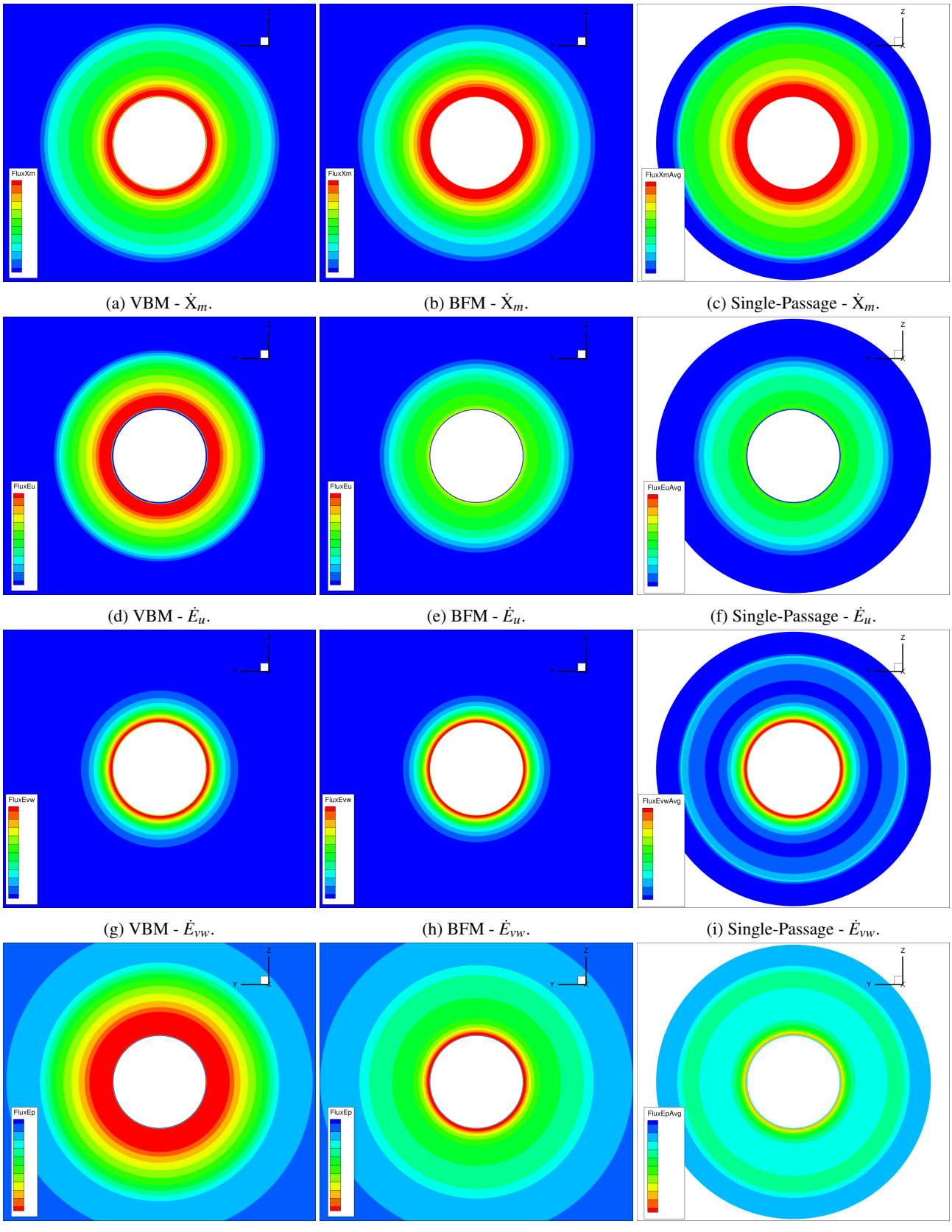

(a) VBM - $\dot{\mathrm{X}}_m$. (b) BFM - $\dot{\mathrm{X}}_m$. (c) Single-Passage - $\dot{\mathrm{X}}_m$.

(d) VBM - $\dot{E}_u$. (e) BFM - $\dot{E}_u$. (f) Single-Passage - $\dot{E}_u$.

(g) VBM - $\dot{E}_{vw}$. (h) BFM - $\dot{E}_{vw}$. (i) Single-Passage - $\dot{E}_{vw}$.

(j) VBM - $\dot{E}_p$. (k) BFM - $\dot{E}_p$. (l) Single-Passage - $\dot{E}_p$.

Figure 7: Visualisation of the mechanical exergy Flux $\dot{\mathrm{X}}_m$ and its components ($\dot{E}_u$, $\dot{E}_{vw}$, $\dot{E}_p$) on an x_{tp} plane situated downstream of the stator for different modelling approaches. Note that the colormap is inverted for the $\dot{E}_p$ term.

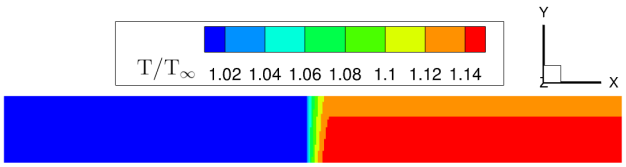

(a) T/T_∞ in the $x-y$ plane.

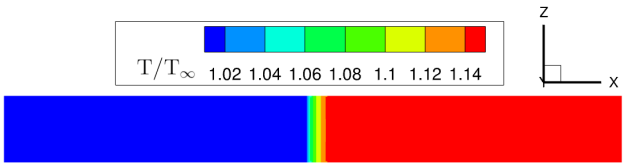

(b) T/T_∞ in the $x-z$ plane.

Figure 8: Visualising the temperature variation across the solution displaying the normalised temperature, T/T_∞.

highlight that the increase in the term $C\dot{X}_{th}$ almost exclusively stems from $C\dot{X}_{th\delta s}$, which is consistent with the source term modeling. In other words, the exergy flux introduced by the heat exchanger in this case is not recoverable by a mechanical device, but rather by a heat engine.

The impact of the operating conditions of the heat exchanger on the exergy balance are also studied. In particular, the influence of the mass flow rate, $\dot{m}$, on the exergy terms and the exergy-based efficiency. The breakdown of the different exergy terms at various mass flow rates is shown in Fig. 11. The terms are displayed in their dimensional form due to the influence of the mass flow rate on the magnitude of the non-dimensional coefficients. The exergy inflow $\dot{X}_{tf}$ introduced by the BFM peaks approximately around the mid operational mass flow rate. Additionally, it shows that as the mass flow rate increases, the $C\dot{X}_{th}$ increases, which is mainly due to its $\dot{X}_{th\delta s}$ component. $\dot{X}_{tr}$ then decreases at higher mass flow rates, which indicates a more significant reduction of $C\dot{X}_{tr}+C\dot{X}_m$ (i.e. higher drag, or equivalently lower $C\dot{X}_{tr}$ for a dead state in at a velocity opposite to that of the aircraft) is perceived in the flow through the source term model. Meanwhile, the $\dot{X}_m$ component decreases with the mass flow rate which is primarily caused by the energy term $\dot{E}_p$. The resolved irreversible losses $\dot{A}_{tot}$ overall show only a slight increase with the mass flow rate. This is because they occur mainly within the channel's boundary layers, the influence of which is of second order of magnitude with respect to the source term effect in this simplified configuration.

Additionally, Fig. 12 displays the exergy-based efficiency of the BFM in the heat exchanger, expressed as $\eta = \dot{X}_{tf}/\dot{E}_{tf}$. This relationship stems from $\dot{E}_{tf} = \dot{X}_{tf} + \dot{A}_{tf}$, with $\dot{E}_{tf}$ being the inflow of energy and $\dot{A}_{tf}$ the inflow of anergy by the source terms. The above efficiency thus describes the theoretically recoverable portion of the energy introduced from the BFM. In other words, it expresses the portion of the energy injected in the flow that is convertible into useful work. The results depict a trend of decreasing η with the mass flow rate for this BFM model. However, the magnitude of $\dot{E}_{tf}$ is significantly greater than $\dot{X}_{tf}$, which results in very low values of η. This is related to the fact that the injected energy is primarily thermal and involves a higher temperature than the dead state one. This efficiency could be affected by the reference temperature for the heat exchange (e.g. ambient or reservoir temperature), so the amount of recoverable energy could be different for different points of the flight envelope. It is however important to note that the portion convertible into useful work would be recoverable by a thermal device, rather than by a mechanical one.

4.4 Conclusion

This result helps in the validation of the exergy balance method for aerothermal applications and is coherent with what one would expect based on the aerothermal modeling employed in the CFD computation. The analysis has enabled to understand the contributions from the different exergy terms on a fundamental configuration before moving to a more complex configuration where terms may be misinterpreted or misunderstood. This is of great importance while considering cases involving strong coupling between mechanical and thermocompressible terms.

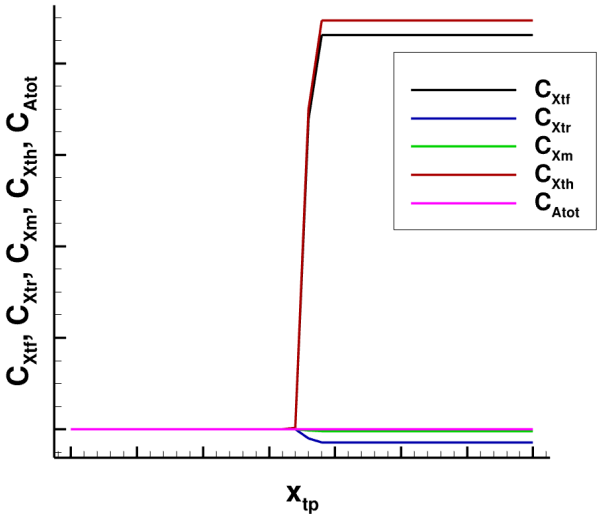

Figure 9: Streamwise evolution of the main terms from the exergy balance for the heat exchanger configuration using the BFM approach.

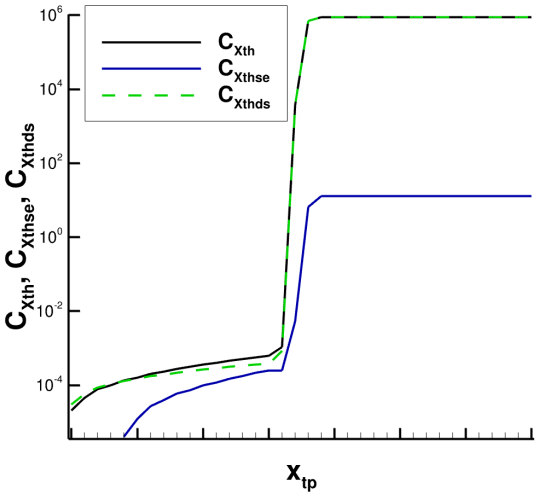

Figure 10: Decomposition of the thermal exergy outflow term, $C\dot{X}_{th}$, into the components $C\dot{X}_{thse} + C\dot{X}_{th\delta s}$ for the heat-exchanger configuration using the BFM approach. Where the y-axis is displayed in logarithmic scale.

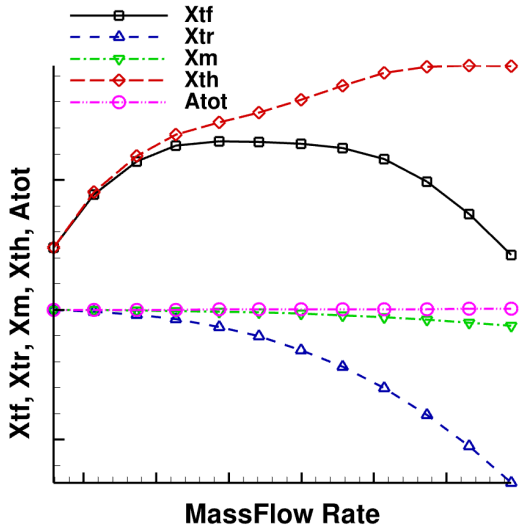

Figure 11: Evolution of the different exergy terms at different massflow rates for the heat exchanger configuration using the BFM.

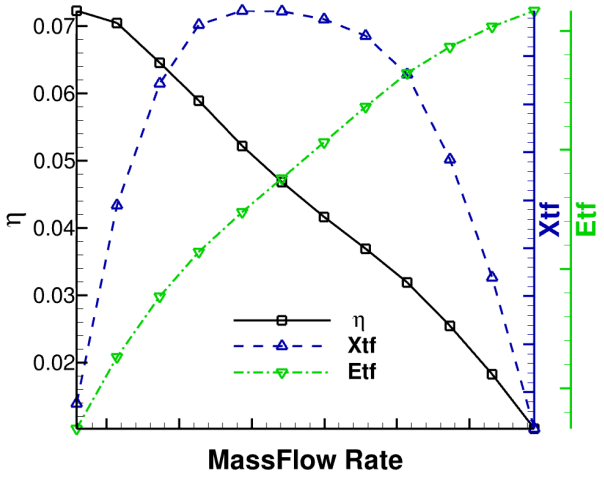

Figure 12: Efficiency, defined as $\eta = \dot{X}_{tf}/\dot{E}_{tf}$, of the BFM at different mass flow rates using the BFM.

5. CONCLUSIONS

This analysis encompasses a comprehensive examination of open fan and heat exchanger configurations, assessing their thermodynamic efficiency and overall performance characteristics. By employing the far-field exergy balance method, this research provides valuable insights into the distribution and utilization of exergy within these complex aerodynamic systems. The detailed breakdown of the exergy balance formulation allows to decompose the effect of different physical phenomena present in the flow and to quantify their influence to overall performance.

Furthermore, the study investigates the impact of various fidelities of modelling approaches and operational parameters on the exergy balance, shedding light on the sensitivities and dependencies that influence the overall efficiency of the examined configurations. Through a systematic approach, the findings contribute to a deeper understanding of the intricacies associated with the interaction between aerodynamic components, compressible effects and thermal processes, thereby informing the design and optimization of future aircraft propulsion systems.

Ultimately, this work aims to enhance our comprehension of the fundamental principles governing the aerodynamic and aerothermal aspects of industrial applications, paving the way for advancements in aircraft technology and contributing to the ongoing efforts toward more sustainable and efficient air transportation.

ACKNOWLEDGEMENTS

The present work was carried out in the frame of the IDEFFIX research project, supported by the French Direc-

torate General for Civil Aviation (DGAC). The studied model open fan geometry was designed by Safran in the frame of the INPRO research project, also supported by DGAC. Both projects were part of the French national Plan de relance, supported by E.U. funding within the NextGeneration EU framework. The development of the elsA software used in part of this work is funded by its co-owners: ONERA, Airbus, and Safran. CODA is the new-generation computational fluid dynamics (CFD) software being developed as part of a collaboration between the French Aerospace Lab ONERA, the German Aerospace Center (DLR), Airbus, and their European research partners. CODA is jointly owned by ONERA, DLR and Airbus.

REFERENCES

[1] Mark Drela. Considerations in aerodynamic force decomposition. In *AIAA Aviation Forum, Paper 2021-2552*, 2021. doi: 10.2514/6.2021-2552.

[2] Aurélien Arntz. *Civil Aircraft Aero-thermo-propulsive Performance Assessment by an Exergy Analysis of High-fidelity CFD-RANS Flow Solutions*. PhD thesis, Lille 1 Université - Sciences et Technologies, Lille, France, 2014. URL https://hal.science/tel-01113135.

[3] Aurélien Arntz, Olivier Atinault, and Alain Merlen. Exergy-based formulation for aircraft aeropropulsive performance assessment: Theoretical development. *AIAA Journal*, 53(6):1627–1639, 2015. doi: 10.2514/1.J053467.

[4] Ilyès Berhouni, Didier Bailly, and Ilias Petropoulos. Exergy balance extension to rotating reference frames: Application to a propeller configuration. *AIAA Journal*, 61(4):1790–1806, 2023. doi: 10.2514/1.J062216.

[5] Ilias Petropoulos, Didier Bailly, Olivier Atinault, Jean-Luc Hantrais-Gervois, Christelle Wervaecke, Jean-Christophe Boniface, Antoine Dumont, Ilyès Berhouni, Simon Trapier, Myles Morelli, Luis Lopez de Vega, William Thollet, Edoardo Paladini, and Alexandre Couilleaux. Overview of the IDEFFIX project towards the development of the far-field exergy balance method at an industrial level of complexity. In *58th 3AF International Conference on Applied Aerodynamics*, Orléans, France, 27-29 March 2024. Paper ID: AERO2024-15.

[6] Ilyès Berhouni, Didier Bailly, and Ilias Petropoulos. On the definition of exergy in the field of aerodynamics. *AIAA Journal*, 51(10):4356–4366, 2023. doi: 10.2514/1.J062833.

[7] Daniel Destarac. *Far-Field / Near-Field Drag Balance and Applications of Drag Extraction in CFD, In: CFD-based Aircraft Drag Prediction and Reduction*. VKI Lecture Series 2003. Von Karman Institute for Fluid Dynamics, Rhode Saint Genèse, February 3-7, 2003, National Institute of Aerospace, Hampton (VA), November 3-7, 2003.

[8] Jaap van der Vooren and Daniel Destarac. Drag/thrust analysis of jet-propelled transonic transport aircraft; definition of physical drag components. *Aerospace Science and Technology*, 8(6): 545–556, 2004. doi: 10.1016/j.ast.2004.03.004.

[9] Didier Bailly, Ilias Petropoulos, Christelle Wervaecke, Michaël Méheut, Olivier Atinault, and Camille Fournis. An overview of ONERA research activities related to drag analysis and breakdown. In *AIAA Aviation Forum, Paper 2021-2551*, 2021. doi: 10.2514/6.2021-2551.

[10] Miguel Ángel Aguirre. *Exergy analysis of innovative aircraft with aeropropulsive coupling*. PhD thesis, Université de Toulouse, 2022.

[11] Ilyès Berhouni. *Theoretical study of the exergy balance method and extension to the performance analysis of steady rotating flows*. PhD thesis, Institut Polytechnique de Paris, France, 2023. NNT: 2023IPPAX131.

[12] Ilyès Berhouni, Ilias Petropoulos, and Didier Bailly. Exergetic analysis of the NASA rotor 37 compressor test case. In *15th European Conference on Turbomachinery Fluid dynamics & Thermodynamics (ETC15), Budapest, Hungary*, April 24-28, 2023. URL https://hal.science/hal-04099251. Paper ID: ETC2023-171.

[13] Ilyès Berhouni, Didier Bailly, and Ilias Petropoulos. Exergy balance decomposition between mechanically- and thermally-recoverable exergy outflows. *AIAA Journal*, 2024. doi: https://doi.org/10.2514/1.J063118. Article in advance.

[14] Christophe Benoit, Stéphanie Péron, and Sâm Landier. Cassiopee: a CFD pre-and post-processing tool. *Aerospace Science and Technology*, 45:272–283, 2015. doi: 10.1016/j.ast.2015.05.023.

[15] Laurent Cambier, Sébastien Heib, and Sylvie Plot. The Onera elsA CFD software: input from research and feedback from industry. *Mechanics & Industry*, 14(3):159–174, 2013. doi: https://doi.org/10.1051/meca/2013056.

[16] Pedro S. Volpiani, Jean-Baptiste Chapelier, Axel Schwöppe, Jens Jägersküpper, and Steeve Champagneux. Simulating the Common Research Model

using the new CFD software from ONERA, DLR and Airbus. In *AIAA Aviation Forum 2023*, 12-16 June 2023. doi: 10.2514/6.2023-3275. Paper ID: AIAA 2023-3275.

[17] William Thollet, Guillaume Dufour, Xavier Carbonneau, and Florian Blanc. Body-force modeling for aerodynamic analysis of air intake–fan interactions. *International Journal of Numerical Methods for Heat & Fluid Flow*, 26(7):2048–2065, 2016. ISSN 0961-5539. URL https://doi.org/10.1108/HFF-07-2015-0274.

[18] Stefano Wahono. Development of virtual blade model for modelling helicopter rotor downwash in openfoam. Technical Report DSTO-TR-2931, Australian Government Department of Defence, 2013.